

Magneto-Thermal Analysis of Induction Heating Processes

F. Freschi¹, L. Giaccone¹ and M. Repetto¹

Abstract: The study of induction heating systems from the electromagnetic point of view is still a challenging task for several reasons: the problem under analysis is strictly multiphysics because it involves the coupled electromagnetic and thermal phenomena; both coupled physics have nonlinear behavior; nonlinearities are of different kinds, both depending on the single phenomenon and on the coupling terms. The aim of the paper is to show that the cell method, based on the use of Tonti diagrams, can handle efficiently this kind of problems. The proposed magneto-thermal numerical procedure is firstly described in its theoretical aspects and then it is applied to a numerical benchmark. Comparisons are carried out with a commercial software on the single physic problem and then the complete coupled analysis is performed.

Keywords: Cell method, coupled problems, induction heating, magneto-quasistatic, nonlinear problems.

1 Introduction

The analysis of multiphysics problems is becoming nowadays more and more important. The design requests for many industrial products are tough so that approximate analyses performed on a single physic basis are not sufficient to guarantee the final acceptance of the design. For instance thermal effects, that were usually neglected or weakly coupled in the design of many electromagnetic devices, must now be strongly coupled with their electromagnetic counterparts. The finite element method is the gold-standard numerical method used to this aim. Coupled analysis by finite element procedures are available in many commercial tools but they are often based on a weak coupling between single physic solvers. The sequential data exchange is then needed for the coupling. The use of numerical formulations directly related to the physical variables involved in the problems, makes it possible a more efficient coupling among different physics.

¹ Dipartimento Energia, Politecnico di Torino, corso Duca degli Abruzzi, 24, 10129 Torino.

The use of Tonti diagrams [Tonti (2001)] exploits a common framework among different physical phenomena [Delprete, Freschi, Repetto, and Rosso (2009, 2010)]. The Tonti formalism is based on the classification of the rules and of the variables involved in many mathematical models: elastostatics [Tonti and Zarantonello (2009)], elastodynamics [Tonti and Zarantonello (2010)], crack theory [Ferretti (2003, 2009)], unsaturated flow through porous media Straface, Troisi, and Gagliardi (2006)], electrostatics [Bettini and Trevisan (2003)], magnetostatics [Repetto and Trevisan (2004)], eddy currents [Specogna and Trevisan (2005)] and full Maxwell problems [Alotto, De Cian, and Molinari (2006)] are only a few examples of the many physical theories classified into this structure. Rules governing the phenomenon are subdivided in topological and constitutive equations. Examples of the first ones are the balance equations relating, for instance, the heat flow on the surface of a volume to the heat produced inside the volume. These equations are not specific of a particular phenomenon but are more related to the properties of space and of its tessellation. Constitutive equations involve the properties of the media in which the phenomena is taking place and again are common to many phenomena like the Fourier equation in heat transmission or the elastic equation in structural problems. Starting from these considerations, basic topological operators are introduced and they can be interpreted as the discrete counterpart of the differential operators: gradient along a line can be expressed as a difference between nodal values on the edges extrema, divergence operator is related, by means of Gauss theorem, to the flow of a vector quantity on the surface bounding a volume etc.. These operators are shared by different phenomena described by the same space discretization and thus a multiphysics study takes advantage of this common ground [Alotto, Freschi, and Repetto (2010); Moro, Alotto, Freschi, and Guarneri (2012)]. Another reason that makes the use of Tonti formalism more adapt for multiphysics is relevant to the type of variables used: in the Tonti formulations variables are of the global kind, that is variables associated to space elements, for instance an electro-motive force along a line, a flux on a surface etc.. These variables have a physical meaning in the sense that they can be usually measured. Their physical meaning helps the coupling of different phenomena making available, in one formulation, the linking term needed in another: for instance the power dissipated in one volume for electromagnetic reasons can be directly given in input to a thermal analysis without the need of any further computation or interpolation.

Global variables are then associated with oriented space-time geometrical entities. Two discretizations are defined over the problem domain: the usual discretization adopted by many numerical methods forms a complex of space elements called *primal complex* but another cell complex is also defined, which is intertwined with the primal one by duality relations. Thus dual volumes are one-to-one associated to

primal nodes, dual faces are dual geometrical entities of primal lines, dual lines of primal faces and dual points of primal volumes. Depending on their nature, global variables are associated to the primal or dual complex [Tonti (2002)].

Following this line of reasoning, a set of Matlab functions have been developed and collected in a computational tool named DualLab [Freschi, Giaccone, and Repetto (2008)]. Particular attention has been devoted at the implementation of the previously highlighted peculiarities: starting from a geometric tessellation based on hexaedra or tetrahedra, the dual mesh, topological operators and constitutive matrices are created. Thank to the advanced linear algebra capabilities provided by Matlab, matrices can be easily combined to obtain the final system.

In this paper, the solution of the magneto-thermal problem related to the induction heating process is presented, the coupled formulation is described and the treatment of the main problems related to the nonlinearities present in the phenomena are discussed. The formulation is compared with a commercial code in a simplified problem and finally the full coupled nonlinear solution is discussed.

2 Induction heating

Induction heating is the industrial process used to transfer heating power to a conductive workpiece with eddy currents [Davies (1990)]. Even if different applications can be found ranging from the melting of materials to their forming, the heating conditions obtained by magnetic induction are particularly well suited to transfer heating power on the surface of the workpiece and thus it can be efficiently used for hardening and quenching treatment. From a numerical point of view, several challenging problems are encountered [Freschi and Repetto (2012)]. They are briefly outlined in the next sections.

2.1 Spatial distribution of currents and problem discretization

In order to increase the power density transferred to the treated material, inductors are supplied with high frequency currents, usually in the range of 1 – 100 kHz. Because of these frequency values, the penetration depth is usually in the order of a few millimeters on workpieces whose overall dimensions can be a couple of order of magnitudes larger. From a numerical point of view this fact compels the use of a fine spatial discretization close to surface [Canova, Dughiero, Fasolo, Forzan, Freschi, Giaccone, and Repetto (2009a)]. In addition the Joule power losses are concentrated in this thin layer so that also the thermal problem is discretized with the same spatial accuracy.

2.2 *Nonlinear effects*

In the case of the thermal treatment of ferromagnetic materials, the effects of magnetic nonlinearities cannot be neglected. The high spatial concentration of the magnetic field on the workpiece surface leads to high saturation levels of the magnetic material close to its surface. Magnetic nonlinearity plays a crucial role in the power transfer from the induction system to the workpiece: the magnetic saturation decreases the effective magnetic permeability value of the ferromagnetic material and thus increases the penetration depth of induced eddy currents, and locally reduces the transferred power density.

In addition to the previous effect, ferromagnetic characteristics are also depending on the temperature [Favennec, Labbe, Tillier, and Bay (2002)]: ferromagnetic effects and high value of magnetic permeabilities fall off from the ambient temperature and disappear completely when the temperature value rises above the Curie temperature, around 760 °C for iron. This nonlinear effect strictly links the magnetic and thermal problems. The disappearance of ferromagnetism changes the eddy current and power distributions along the workpiece.

Besides the cited magnetic nonlinearities, also other characteristics of the medium experience variation of their parameters as function of the temperature. A part from the value of electrical and thermal conductivities, that decrease their values when the temperature rises, another nonlinear effect is related to the phase change of the ferromagnetic material around the Curie temperature. This phase transition involves a latent heat. In fact, during this transition, the system either absorbs or releases an amount of energy that changes its internal energy status without changing the temperature of the system that remains constant as heat is added. This well known phenomenon is taken into account by considering a temperature dependent heat capacity, whose value is larger during the phase change. The value of this fictitious heat capacity is tuned in order to be equal to the latent heat involved in the process.

2.3 *Time scales of the magnetic and thermal phenomena*

Notwithstanding the strong coupling of the magnetic and thermal effects, their time dynamics are quite different: magnetic phenomena are driven by the supply frequency: at 1 kHz the time discretization is around tens of microseconds. On the other hand, thermal effects are ruled by the time constant of the heat transmission that is usually in the range of 1 ÷ 10 s. This peculiarity could be exploited for an optimal management of the two coupled problems: while magnetic problems must be treated on a milliseconds or less scale, temperature values at this scale can be considered almost as constant and could be updated on a larger time scale. In

the present case two different dynamic formulations are adopted: nonlinear time-harmonic for the magnetic problem and time-stepping for the thermal problem.

3 Magneto-thermal coupled formulation

The magnetic problem was already worked out in [Canova, Dughiero, Fasolo, Forzan, Freschi, Giaccone, and Repetto (2009b)] in which a complete solution obtained by means of a commercial code, was compared with an approximate method that decoupled the three dimensional geometric complexity and the heavy saturation effects. The proposed method showed to be effective in the solution of the problem, but the computational time was not compatible with a coupled magneto-thermal simulation. The aim of this section is to overcome these limitations, to exploit the different time scales between the thermal (seconds) and magnetic problem (tens of microseconds) and to improve the convergence of the nonlinear magnetic scheme by taking into account the thermal dependent physical characteristics.

3.1 Eddy current numerical formulation

The eddy current problem is formulated in frequency domain. Several formulations have been proposed in the literature for eddy current problems in finite element context [Bíró, Preis, and Richter (1995)], and most of them have also been proposed accounting to the algebraic scheme [Specogna and Trevisan (2005, 2008)].

Table 1: Global variables for electromagnetic fields.

global variable	SI unit	definition	grid	element
voltage	V	$e = \int \vec{E} \cdot d\vec{l}$	primal	line
line integral of \vec{A}	Wb	$a = \int \vec{A} \cdot d\vec{l}$	primal	line
magnetic flux	Wb	$b = \int \vec{B} \cdot d\vec{S}$	primal	face
magneto-motive force	A	$h = \int \vec{H} \cdot d\vec{l}$	dual	line
current	A	$j = \int \vec{J} \cdot d\vec{S}$	dual	face

The global variables associated to the Maxwell's equations are summarized in Table 1. When global variables are used, physical equations can be written in a discrete form. The discrete operators that are representative of gradient, curl and divergence operators are the incidence matrices \mathbf{G} (edge-to-node), \mathbf{C} (face-to-edge), \mathbf{D} (volume-to-face). Since the same spatial entities are present in the dual complex,

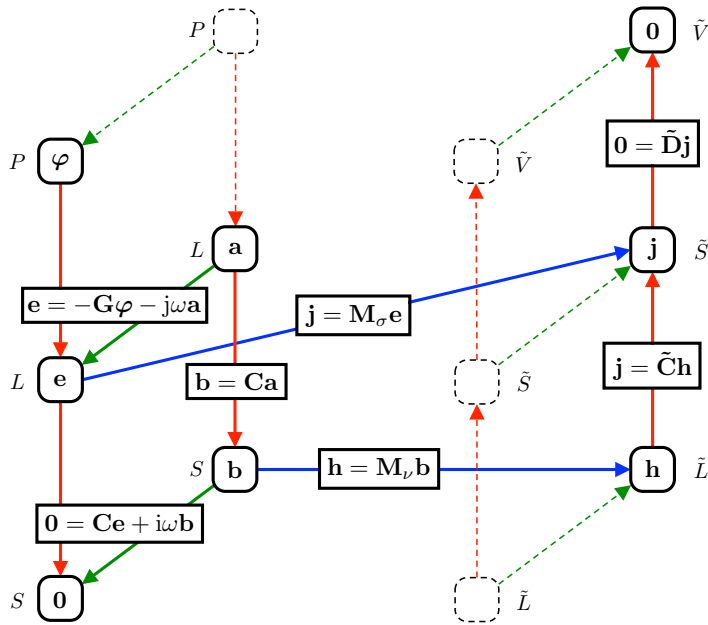


Figure 1: Tonti diagram of Maxwell's equation for magneto-quasi-stationary formulation in steady-state conditions.

similar incidence matrices can be defined for the dual complex. They are represented by a tilde sign: $\tilde{\mathbf{G}}$, $\tilde{\mathbf{C}}$, $\tilde{\mathbf{D}}$. At least for topologically trivial complexes of cells, duality relations impose that:

$$\tilde{\mathbf{D}} = -\mathbf{G}^T \tag{1}$$

$$\tilde{\mathbf{C}} = \mathbf{C}^T \tag{2}$$

$$\tilde{\mathbf{G}} = \mathbf{D}^T \tag{3}$$

Considering the Tonti diagram of time harmonic quasi stationary Maxwell's equations represented in Fig. 1, the topological equations are¹:

$$\mathbf{C}\mathbf{e} = -i\omega\mathbf{b} \tag{4}$$

$$\mathbf{b} = \mathbf{C}\mathbf{a} \tag{5}$$

$$\tilde{\mathbf{C}}\mathbf{h} = \mathbf{j} + \mathbf{j}_s \tag{6}$$

¹ here the common phasor notation is omitted for the sake of simplicity.

$$\tilde{\mathbf{D}}\mathbf{j} = \mathbf{0} \quad (7)$$

in which \mathbf{j}_S represents the source current vector. Equations that link a quantity defined on the primal complex and another on the dual complex are called constitutive equations and can be represented by square matrices due to the duality of the complexes. In the magnetic quasi-stationary regime, the reluctivity \mathbf{M}_v , and conductivity \mathbf{M}_σ , matrices are introduced [Codecasa, Specogna, and Trevisan (2008)]:

$$\mathbf{h} = \mathbf{M}_v \mathbf{b} \quad (8)$$

$$\mathbf{j} = \mathbf{M}_\sigma \mathbf{e} \quad (9)$$

From a numerical point of view it is convenient to introduce from (4) the reduced magnetic vector potential \mathbf{a}^* as:

$$\mathbf{b} = \mathbf{C} \left(-\frac{\mathbf{e}}{i\omega} \right) = \mathbf{C}\mathbf{a}^* \quad (10)$$

Substituting (10) in (6) and using the material relations (8) and (9), the final system is:

$$(\mathbf{C}^T \mathbf{M}_v \mathbf{C} + i\omega \mathbf{M}_\sigma) \mathbf{a}^* = \mathbf{j}_S \quad (11)$$

The formulation is ungauged and therefore is singular. If the right hand side is divergence free, the system is consistent and can be solved using specialized iterative solvers for complex symmetric systems [Clemens, Weiland, and van Rienen (1998)]. When direct solvers are used, the vector potential \mathbf{a}^* in (11) must be explicitly gauged [Alotto, Freschi, Repetto, and Rosso (2013)].

Induction heating system are characterized by inductors whose currents are imposed by electronic power supply systems. A correct modelling requires an integral constraint in order to impose the total current through the source conductors. The implementation of source coils with an impressed current must include an integral constraint on a conductor cut set. This constraint is imposed by means of the topological matrix \mathbf{Q} that identifies the primal edges (dual faces) of the cut set:

$$\mathbf{Q}^T \mathbf{j} = j_0 \quad (12)$$

An unknown fictitious voltage e_0 is applied to the cut edges [De Gersem and Weiland (2004)]:

$$\mathbf{j} = \mathbf{M}_\sigma (\mathbf{e} + \mathbf{Q}e_0) \quad (13)$$

This formulation offers the advantage of keeping the final system symmetric.

$$\begin{bmatrix} \mathbf{C}^T \mathbf{M}_v \mathbf{C} + i\omega \mathbf{M}_\sigma & -\mathbf{M}_\sigma \mathbf{Q} \\ -\mathbf{Q}^T \mathbf{M}_\sigma & \frac{1}{i\omega} \mathbf{Q}^T \mathbf{M}_\sigma \mathbf{Q} \end{bmatrix} \begin{bmatrix} \mathbf{a}^* \\ e_0 \end{bmatrix} = \begin{bmatrix} \mathbf{j}_S \\ \frac{1}{i\omega} j_0 \end{bmatrix} \quad (14)$$

3.1.1 Magnetic nonlinearity

The magnetic nonlinearity creates a distortion of local waveforms of fields, for instance if a sinusoidal waveform of magnetic field is applied and its values are driving the ferromagnetic material into saturation, the resulting magnetic flux variation in time is still periodic but not sinusoidal anymore. Two exact approaches to the solution of this problem can be devised: nonlinear time-stepping technique or harmonic balance scheme. With the first method, the time axis is discretized and the numerical solution is obtained by a time-marching scheme where for each time step a nonlinear problem is solved. This approach must handle a transient phase of the phenomenon and the steady state condition is reached after some time periods. The harmonic balance approach starts from the assumption that the solution is a time-periodic distorted waveform thus using its harmonic decomposition the steady state is computed [Chiampi, Negro, and Tartaglia (1983)].

Besides these two exact approaches, a simplification of the problem can be defined by substituting an equivalent material that, under a sinusoidal excitation, gives the same response of the actual nonlinear material in terms of coenergy [Paoli, Bíró, and Buchgraber (1998)]. This approach [Demerdash and Gillott (1974); Vassent, Meunier, and Sabonnadier (1989)], substitutes to the nonlinear ferromagnetic material an equivalent $B(H)$ characteristic, based on a coenergy equivalence. The time solution is imposed to be harmonic by considering a linear ferromagnetic material whose permeability, however, changes point by point depending on its magnetic flux density level. In each point the permeability is nonlinear, but the working point on the characteristic depends on the peak value of the magnetic flux density sine wave and not on its instantaneous value.

For any $B(H)$ characteristic, the coenergy that corresponds to the magnetic field H^* is defined as:

$$w'(H^*) = \int_0^{H^*} B(H) dH \tag{15}$$

A coenergy equivalent material can be defined as the material that, for a given value of H^* , gives rise to the same value of coenergy defined in (15). The constraint can be expressed as:

$$\frac{1}{2} B^* H^* = w'(H^*) \Rightarrow B^* = \frac{2w'(H^*)}{H^*} \tag{16}$$

As it can be seen in Fig. 2, the value of B^* that satisfies the constraint of (16), is such that the coenergy value, given by the union of areas A and B is equal to the area of triangle given by the union of areas A and C . This fact implies that areas B

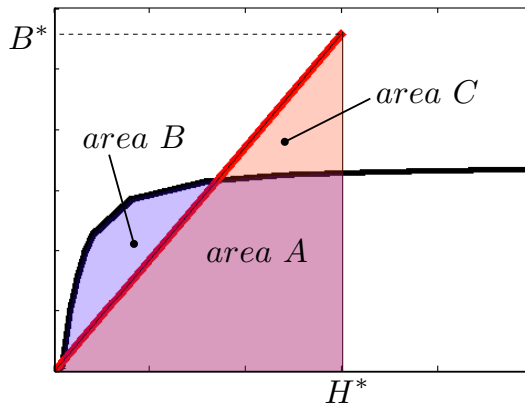


Figure 2: Linear material with (H^*, B^*) having the same coenergy of the nonlinear one.

and C are equal. The resulting value of B^* that satisfies the constraint is larger than the physical magnetic flux density $B(H^*)$.

The previously defined coenergy equivalent material, is computed on a point wise base: for each value of H^* an equivalent B^* is computed. When a periodic field is imposed, the coenergy equivalent concept can be applied to impose the average value of coenergy during the period to be equal in nonlinear and equivalent case. The equivalent time-varying formulation can be defined as: given a nonlinear characteristic (H, B) , define an equivalent material whose nonlinear characteristic (H_{eq}, B_{eq}) gives in one time period the same average coenergy value of the original material excited with a sinusoidal waveform of $H(t)$.

In Fig. 3, the equivalent characteristic of the ferromagnetic material used in the present study is reported. The definition of these equivalent material properties transforms a nonlinear magnetic problem into an inhomogeneous linear one. The material characteristics can be iteratively updated through standard nonlinear schemes (fixed-point, Newton-Raphson). Since the Newton-Raphson technique shows a lack of accuracy in high saturation regions [Chiampi, Chiarabaglio, and Repetto (1994)], nonlinearities are taken into account by using the fixed-point polarization method in the time harmonic regime.

Following this approach, a linearization term (\mathbf{h}_{FP}) is added to the magnetic char-

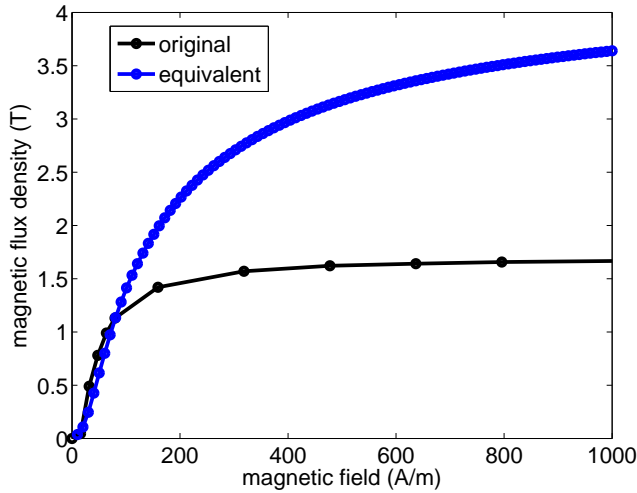


Figure 3: Original and equivalent sinusoidal average $B(H)$ curves.

acteristic [Hantila (1999)]:

$$\begin{bmatrix} \mathbf{C}^T \mathbf{M}_V \mathbf{C} + i\omega \mathbf{M}_\sigma & -\mathbf{M}_\sigma \mathbf{Q} \\ -\mathbf{Q}^T \mathbf{M}_\sigma & \frac{1}{i\omega} \mathbf{Q}^T \mathbf{M}_\sigma \mathbf{Q} \end{bmatrix} \begin{bmatrix} \mathbf{a}^* \\ e_0 \end{bmatrix} = \begin{bmatrix} \mathbf{j}_S - \mathbf{C}^T \mathbf{h}_{FP} \\ \frac{1}{i\omega} \mathbf{j}_0 \end{bmatrix} \quad (17)$$

3.2 Unstationary thermal problem

The unstationary thermal problem makes use of the global variables defined in Table 2. Considering the Tonti diagram of Fig. 4, two topological equations are observed:

$$\mathbf{p} = \frac{d\mathbf{u}}{dt} + \tilde{\mathbf{D}}\Phi \quad (18)$$

$$\gamma = \mathbf{G}\mathbf{T} \quad (19)$$

Primal and dual variables are linked by the thermal capacitance $\mathbf{M}_{\rho c}$ and thermal conductivity \mathbf{M}_λ matrices. Hence, the constitutive equations are:

$$\mathbf{u} = \mathbf{u}_0 + \mathbf{M}_{\rho c} \mathbf{T} \quad (20)$$

$$\Phi = -\mathbf{M}_\lambda \gamma \quad (21)$$

The combination of equations (18) to (21) leads to the formulation of the transient thermal problem:

$$\mathbf{M}_{\rho c} \frac{d\mathbf{T}}{dt} + \mathbf{G}^T \mathbf{M}_\lambda \mathbf{G} \mathbf{T} = \mathbf{p} \quad (22)$$

Table 2: Global variables for unstationary thermal fields, being q the thermal flux density (W/m^2) and w the specific thermal power production (W/m^3).

global variable	SI unit	definition	grid	element
temperature	K	T	primal	point
temperature difference	K	$\gamma = \int \nabla T \cdot \vec{dl}$	primal	line
internal energy	J	u	dual	volume
thermal flux	W	$\Phi = \int q \cdot \vec{dS}$	dual	face
thermal power production	W	$p = \int w dV$	dual	volume

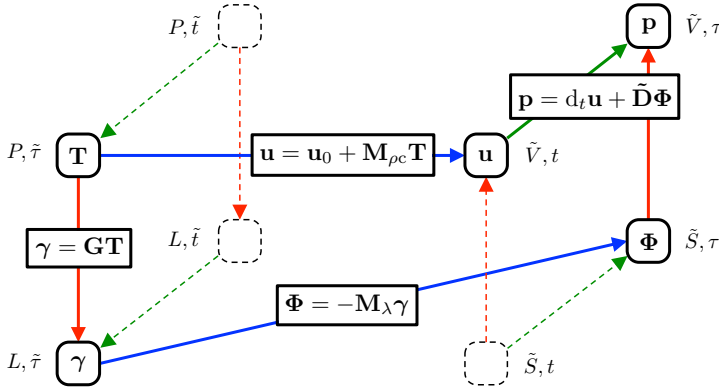


Figure 4: Tonti diagram of unstationary heat transfer.

The ordinary differential equation is discretized using the Crank-Nicolson method. The system is nonlinear, since the physical properties of the materials are temperature dependent, but are considered constant in each time step.

3.3 Coupling terms

The first term of nonlinear coupling between thermal and electrical problems refers to the dependance of the electrical and thermal conductivities on the temperature.

The dependance can be expressed by the equation:

$$\sigma(T) = \frac{\sigma_0}{1 + \alpha_T(T - T_0)} \tag{23}$$

in which σ_0 is the conductivity at the reference temperature and α_T is the temperature coefficient. From the physical point of view, the transition from magnetic to

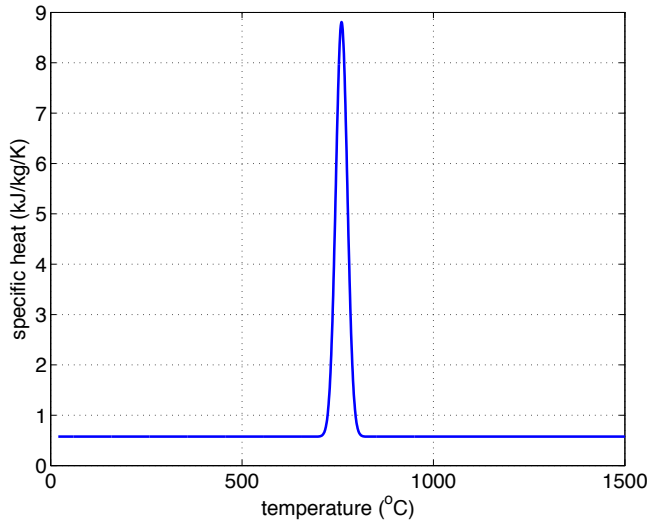


Figure 5: Specific thermal capacity vs. temperature in proximity of the Curie point.

amagnetic characteristic around the Curie temperature requires a latent heat, that is, part of the generated heat is necessary to establish the phase transition. Numerically, this effect is taken into account in the model through a specific thermal capacity that depends on the temperature: across the Curie temperature, the specific thermal capacity increases in order to allow the material to store energy. A typical curve is represented in Fig. 5.

Another source of nonlinearity is constituted by the temperature dependence of the ferromagnetic properties. In fact, when the temperature goes beyond the Curie value, the magnetic material loses its magnetic property and becomes amagnetic. The transition is not abrupt and it is modelled as follows (Fig. 6):

$$B = \mu_0 H + k_T (B_0(H) - \mu_0 H) \quad (24)$$

Equation (24) shows that $k_T = 1$ at low temperatures, while k_T approaches to zero for high temperatures. The effect of the temperature coefficient k_T on a typical $B(H)$ characteristic is shown in Fig. 7. It is clear that beyond the Curie point the magnetic characteristic is that of air.

The last coupling term is due to the power generated by the eddy currents which represents the source of the thermal problem. Using first-order edge shape func-

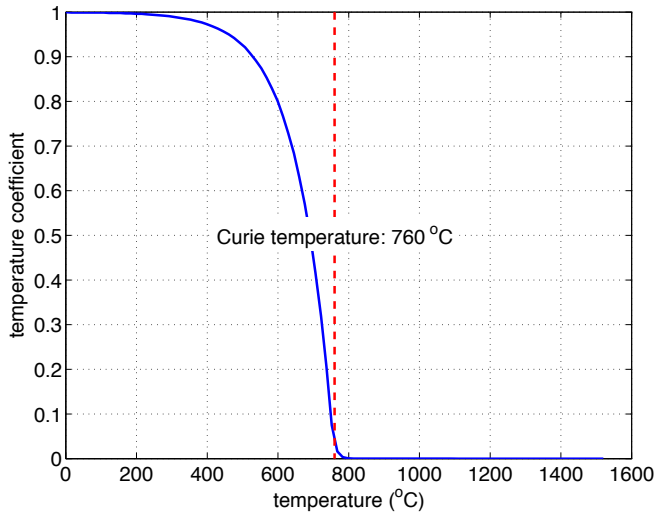


Figure 6: Temperature coefficient for $B(H)$ curve.

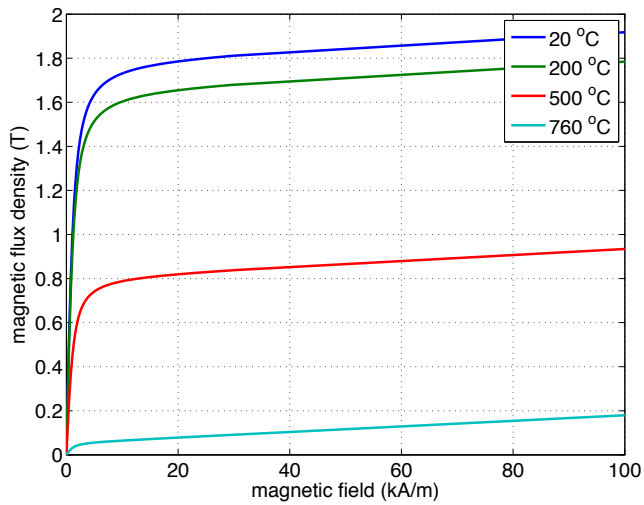


Figure 7: $B(H)$ characteristics at different temperatures.

tions \vec{w} to interpolate the electric field \vec{E} , the power losses in each simplex m are:

$$\begin{aligned} \int_{V_m} \vec{E} \cdot \vec{J} dV &= \int_{V_m} \left(\sum_k e_k \vec{w}_k \right) \cdot \vec{J} dV \\ &= \sum_k e_k \int_{V_m} \vec{w}_k \cdot \vec{J} dV. \end{aligned} \tag{25}$$

The integral in (25) gives the electric current j'_k . By assuming a uniform current density inside the element:

$$j'_k = \vec{J} \cdot \int_{V_m} \vec{w}_k dV. \tag{26}$$

Since the integral in (26) equals the k th dual face area vector, as shown in Lemma 1 of [Bossavit (2000)]:

$$\int_{V_m} \vec{w}_k dV = \vec{S} \tag{27}$$

one obtains:

$$\int_{V_m} \vec{E} \cdot \vec{J} dV = \sum_k e_k j'_k \tag{28}$$

where V_m is the volume of the simplex, e_k is the voltage defined across the k th primal edge and j'_k is the portion of the current defined on the k th dual surface that belongs to the m th simplex. Equation (28) shows that the power in each element can be evaluated starting from global quantities which are directly available in the cell method. All the powers defined for each primal edge/dual face couple can be collected in a vector \mathbf{p}_E

$$\mathbf{p}_E = \mathbf{e} \circ \mathbf{j} \tag{29}$$

where \circ defines the Hadamard element-wise product. Since the thermal formulation requires a heat source to be defined on the dual volumes, these edge-related values have to be projected onto dual volumes.

In order to obtain a matrix-compatible formulation of the coupling term, it is useful to define the support region of the generic k th component of the vector of \mathbf{p}_E . Among the several possibilities, a reasonable choice is to assign the power p_k to the region obtained by connecting the primal edge extrema to the vertices of the corresponding dual face, as shown in Fig. 8 for the case of 2d domains. This region is sometime called trial tessellation. In this case, it is easy to project the powers \mathbf{p}_E

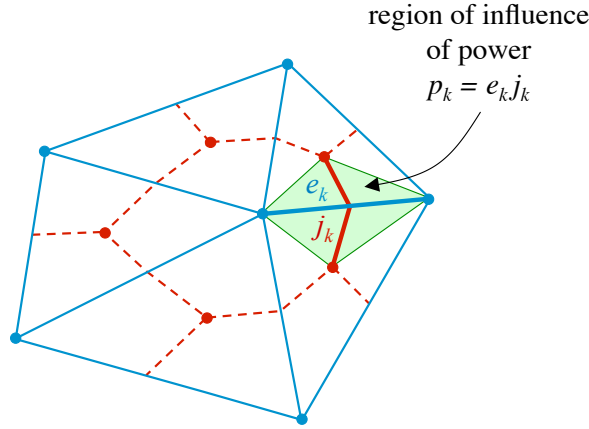


Figure 8: Possible choice for the region of influence of $p_k = e_k j_k$.

onto the dual volumes by using the node-to-edge connectivity matrix \mathbf{G} , since the dual volumes are one-to-one related to the primal nodes:

$$\mathbf{p} = \frac{1}{2} |\mathbf{G}^T| \mathbf{p}_E = \frac{1}{2} |\mathbf{G}^T| \mathbf{e} \circ (\mathbf{M}_\sigma \mathbf{e}) \tag{30}$$

The term $\frac{1}{2}$ is due to the fact that the power related to each primal edge/dual face couple is shared by two adjacent dual volumes.

4 Test case: heating inductor

As shown in Fig. 9 the case study is represented by a single coil that heats up a 1.5 cm thick square metallic plate separated by a gap of 1 mm. In order to increase the coupling between the inductor and the workpiece, a flux concentrator is mounted across the inductor. The inductor is supplied by a sinusoidal current of 2.5 kA at 8 kHz.

4.1 Assessment of the nonlinear magnetic problem

In this section the solution performed by the proposed formulation is compared with a nonlinear solution in time domain obtained with the commercial software CST EM Studio [Computer Simulation Technology AG (2013)]. The steady state of the system is reached after about 20 ms and is practically independent on the source waveform and frequency. In order to speed-up the transient solution, the

frequency is dropped to 300 Hz. With this assumption, the number of time steps is significantly reduced while the properties of the systems are not changed.

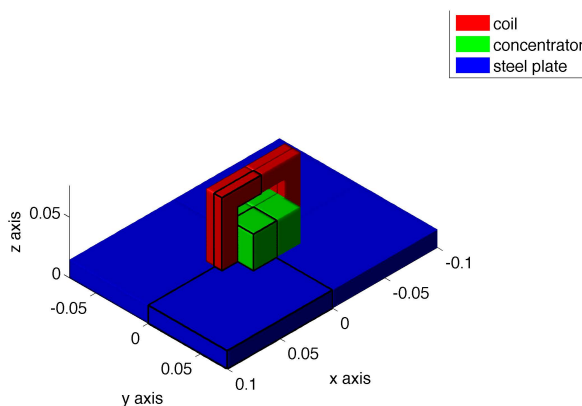


Figure 9: Layout of the case study for the nonlinear magnetic problem. Because of the symmetries, only one-fourth of the model is simulated.

The field quantities are compared in a point belonging to the upper surface of the metallic plate located in the center of the plate, that is, under the center of the inductor. The magnetic flux density induced on the workpiece surface is mainly directed along y direction while the current density is directed along x axis. The time plots of these two quantities are shown in Fig. 10 and Fig. 11, respectively. The magnetic flux and current density waveforms are distorted, while the nonlinear harmonic approach provides equivalent sine waves. As far as the magnetic flux density is concerned, Fig. 10, the coenergy equivalent approximation is not satisfactory. However, results are in accordance with the effective magnetic characteristic, as shown in Fig. 3. On the contrary, a much better agreement is found between the current density curves (Fig. 11).

The most important comparison is on the Joule losses, because they are the sources of the thermal simulation. Fig. 12 shows the instantaneous power, the average power and the real power in the plate calculated by the nonlinear transient solution and the equivalent coenergy approach. A part from the the very first periods, the average power tends asymptotically to the real power calculated by the nonlinear harmonic method. The same conclusions are drawn when looking at the losses in the coil, Fig. 13. From a computational point of view, the nonlinear time domain approach required 17 hours while the time harmonic solver required 9.5 mins on a

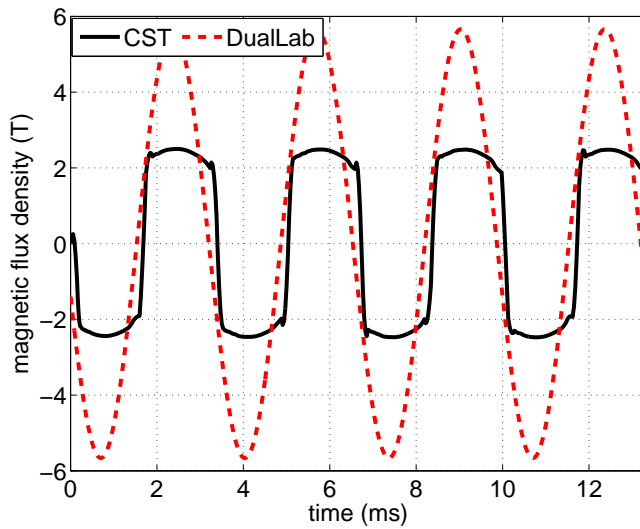


Figure 10: Comparison of the magnetic flux density in a field point located on the surface of the metallic plate under the coil.

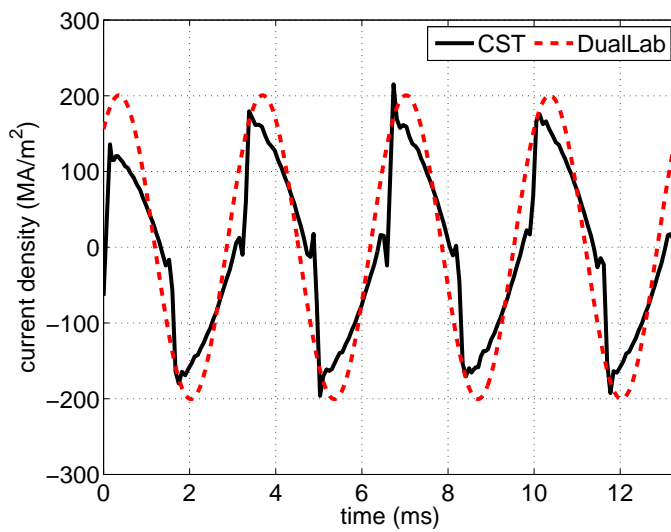


Figure 11: Comparison of the current density in a field point located on the surface of the metallic plate under the coil.

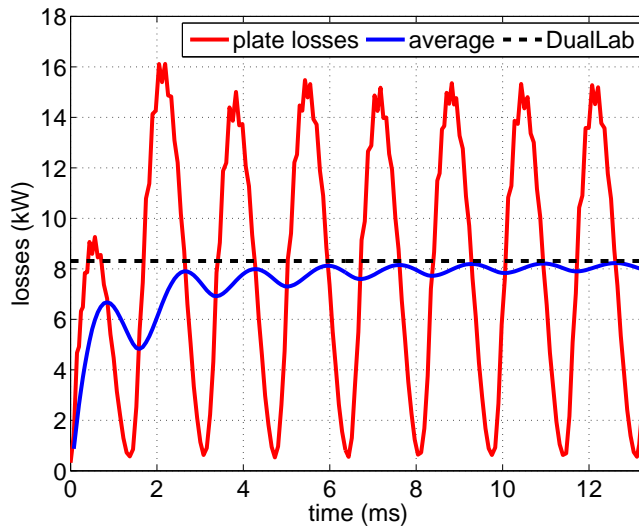


Figure 12: Comparison of the plate losses. The average losses as a function of time are compared with the result obtained by means of DualLab.

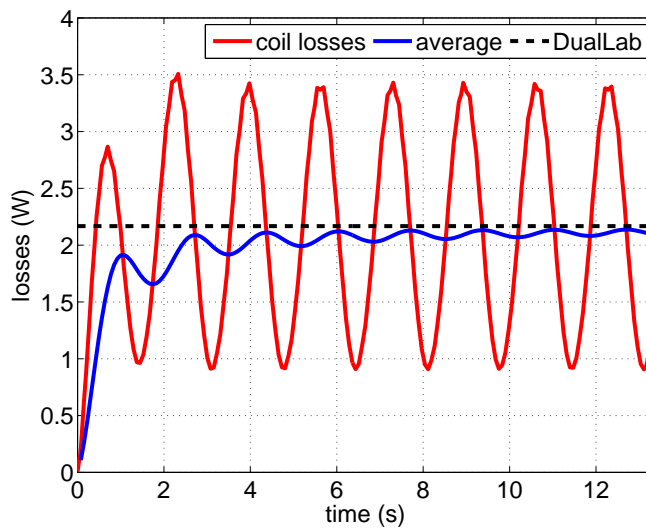


Figure 13: Comparison of the coil losses. The average losses as a function of time are compared with the result obtained by means of DualLab. It is apparent that there is a good agreement.

workstation equipped with two Intel Xeon six-core X5650 at 2.66 GHz and 128 GB of RAM.

The modification of the nonlinear $B(H)$ characteristic with the coenergy equivalent method is a good option for induction heating problems because even if the local quantities are modified, the Joule losses are correctly computed. Since the computation of the thermal transient involves a magnetic simulation at each thermal step, the time harmonic approach is preferred to minimize the overall computational time.

5 Results

The coupled thermo-electromagnetic analysis of the induction heating process is then performed for 10 s. Details of the simulations are reported in Table 3.

Table 3: Computational data for the strong coupled magneto-thermal transient simulation

Phase	Value
No. of nodes (unknowns for the thermal problem)	95472
No. of edges (unknowns for the magnetic problem)	280107
average factorization time (direct solver)	250 s
average nonlinear solution time	435 s
No. of equi-spaced time steps	101
total simulation time	\approx 12 hours

The nonlinear thermal capacitance is demonstrated to be effective in modelling the thermostatic effect during the magnetic transition around the Curie temperature shown in Fig. 14. The effect of high magnetic saturation can be seen in Fig. 15 by looking at the curve for $t = 1$ s. It is also possible to see that heating the workpiece results in a decrease in the apparent relative permeability, and consequently an increase in the penetration depth. The current density penetrates into the workpiece, giving rise to a more uniform temperature distribution (Fig. 16). Finally, Fig. 17 shows the power density maps at different time instants. The effects of the temperature dependent material properties is evidenced in the movement of the hot-spots region on along the workpiece: the higher the temperature, the lower the electric conductivity. Consequently the eddy currents decrease as well.

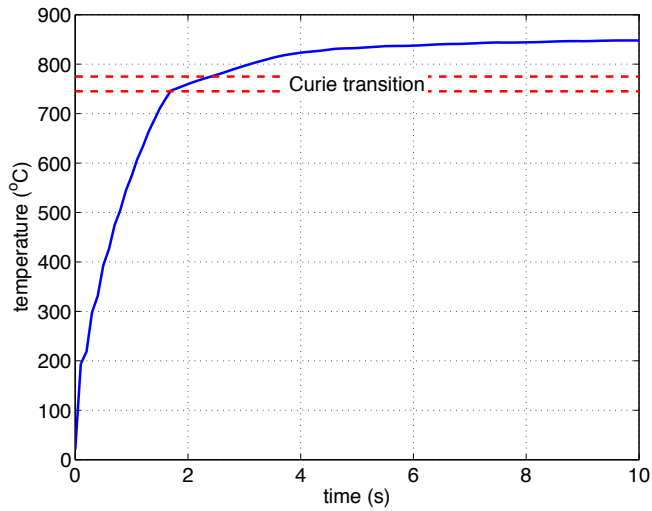


Figure 14: Temperature on workpiece surface.

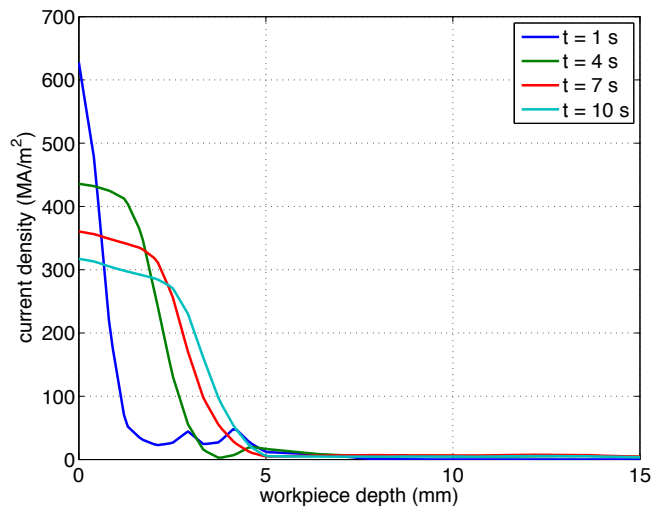


Figure 15: Eddy current density profile along the workpiece depth.

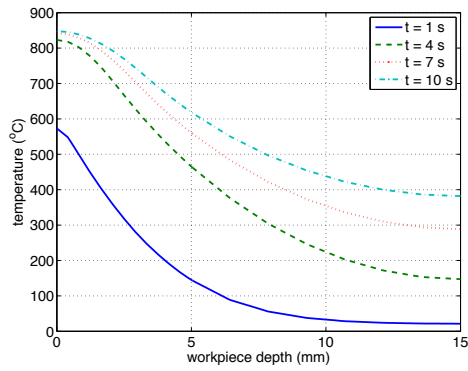


Figure 16: Temperature profile along the workpiece depth.

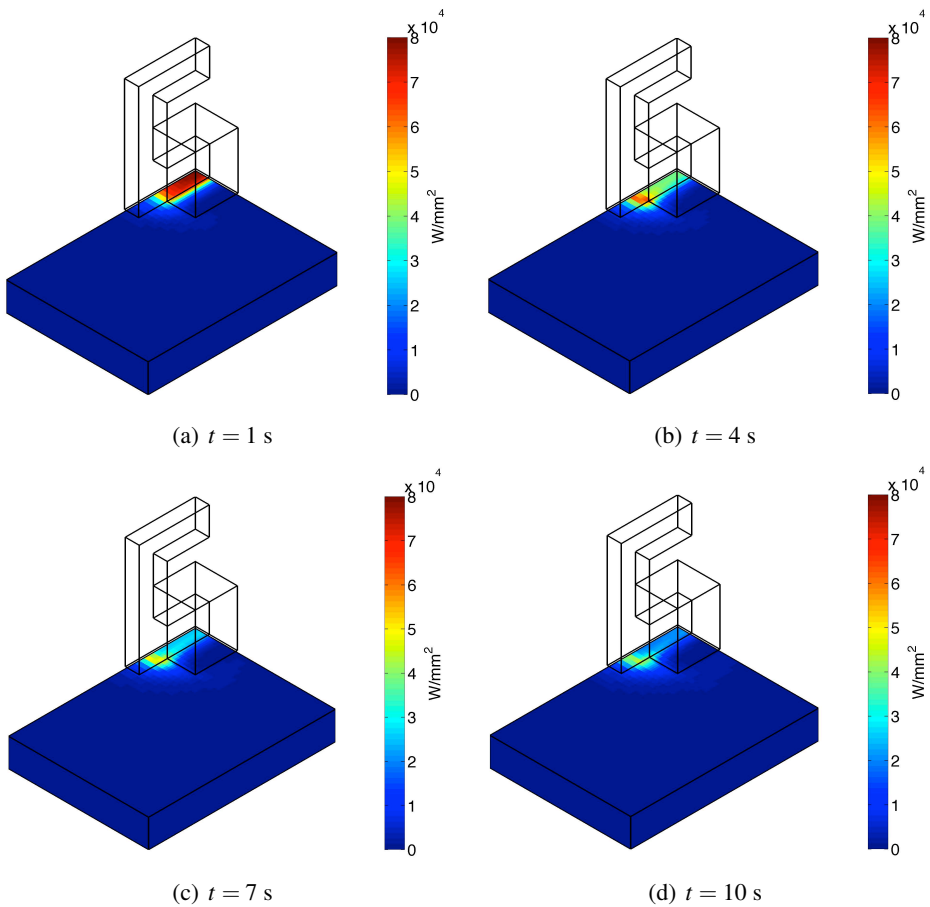


Figure 17: Power density map at different time instants.

6 Conclusions and perspectives

The work performed has highlighted many encouraging aspects of the cell method conforming that it is a numerical technique particularly suited for the analysis of multiphysics problems. As a first remark, the foundation of the cell method on the Tonti diagrams is able to unify, inside a common framework, different physical phenomena. As a second remark, the definition of global variables associated to the geometrical structure and the fact that all physical problems share the same space discretization, makes the coupling of the two single physics formulations straightforward. Finally, the definition of a discrete structure that translates topological and constitutive equations in matrix form makes efficient the use of linear algebra high level languages for the implementation of the numerical procedure.

Following the afore mentioned reasons, a procedure for the study of multiphysics problems have been developed and applied in different application areas. One of these areas regards the analysis of induction heating processes that involves the strict coupling of electromagnetic and thermal phenomena. As it has been already pointed out in this paper, the induction heating is a numerically tough problem: penetration depth of the induced eddy currents is usually a couple of order of magnitudes smaller than the overall dimensions of the problem and, in addition, strong nonlinearities affect all the aspects of the phenomena. The work presented shows that the cell method is able to deal with these kinds of problems and that suited formulations can be easily devised for the solution of the multiphysics configuration. Notwithstanding the common space discretization, time evolution of the two phenomena is treated in two different ways. By taking advantage of the large time evolution differences between electromagnetic and thermal phenomena, particular formulations are adopted: nonlinear time-harmonic for the electromagnetic problem and time stepping for the thermal one. This time solution layout have the advantage of speeding up the solution without losing its peculiarities.

The work is currently ongoing to deduce the micro structural composition of the workpiece after the thermal treatment from the temperature profiles.

References

- Alotto, P.; De Cian, A.; Molinari, G.** (2006): A time-domain 3-D full-Maxwell solver based on the Cell Method. *IEEE Transactions on Magnetics*, vol. 42, no. 4, pp. 799–802.
- Alotto, P.; Freschi, F.; Repetto, M.** (2010): Multiphysics problems via the cell method: The role of tonti diagrams. *IEEE Transactions on Magnetics*, vol. 46, no. 8, pp. 2959–2962.

- Alotto, P.; Freschi, F.; Repetto, M.; Rosso, C.** (2013): *The Cell Method for Electrical Engineering and Multiphysics Problems, An Introduction*. Springer Verlag, Berlin-Heidelberg.
- Bettini, P.; Trevisan, F.** (2003): Electrostatic analysis for plane problems with finite formulation. *IEEE Transactions on Magnetics*, vol. 39, no. 3, pp. 1127–1130.
- Bíró, O.; Preis, K.; Richter, K.** (1995): Various FEM formulations for the calculation of transient 3D eddy currents in nonlinear media. *IEEE Transactions on Magnetics*, vol. 31, no. 3, pp. 1307–1312.
- Bossavit, A.** (2000): Computational electromagnetism and geometry: (5) The “Galerkin hodge”. *Journal of the Japan Society of Applied Electromagnetics*, vol. 8, no. 2, pp. 203–209.
- Canova, A.; Dughiero, F.; Fasolo, E.; Forzan, M.; Freschi, F.; Giaccone, L.; Repetto, M.** (2009): Identification of equivalent material properties for 3-D numerical modeling of induction heating of ferromagnetic workpieces. *IEEE Transactions on Magnetics*, vol. 45, no. 3, pp. 1851–1854.
- Canova, A.; Dughiero, F.; Fasolo, E.; Forzan, M.; Freschi, F.; Giaccone, L.; Repetto, M.** (2009): Simplified approach for 3d nonlinear induction heating problems. *IEEE Transactions on Magnetics*, vol. 45, no. 3, pp. 1855–1858.
- Chiampi, M.; Chiarabaglio, D.; Repetto, M.** (1994): An accurate investigation on numerical methods for nonlinear magnetic field problems. *Journal of Magnetism and Magnetic Materials*, vol. 133, pp. 591–595.
- Chiampi, M.; Negro, A.; Tartaglia, M.** (1983): Alternating electromagnetic field computation in laminated cores. *IEEE Transaction on Magnetics*, vol. 19, no. 4, pp. 1530–1536.
- Clemens, M.; Weiland, T.; van Rienen, U.** (1998): Comparison of krylov-type methods for complex linear systems applied to high-voltage problems. *IEEE Transaction on Magnetics*, vol. 34, no. 5, pp. 3335–3338.
- Codecasa, L.; Specogna, R.; Trevisan, F.** (2008): Discrete constitutive equations over hexahedral grids for eddy-current problems. *Computer Modeling in Engineering & Sciences*, vol. 31, no. 3, pp. 129–144.
- Computer Simulation Technology AG** (2013): CST EM Studio. www.cst.com, 2013.
- Davies, E.** (1990): *Conduction and induction heating*. Institution of Electrical Engineers, London, UK.

De Gersem, H.; Weiland, T. (2004): Field-circuit coupling for time-harmonic models discretized by the finite integration technique. *IEEE Transaction on Magnetics*, vol. 40, no. 2, pp. 1334–1337.

Delprete, C.; Freschi, F.; Repetto, M.; Rosso, C. (2009): Thermo-mechanical analysis using a multiphysics approach. *Journal of Physics: Conference Series*, , no. 181.

Delprete, C.; Freschi, F.; Repetto, M.; Rosso, C. (2010): Experimental validation of a numerical multiphysics technique for electro-thermo-mechanical problem. *The International Journal for Computation and Mathematics in Electrical and Electronic Engineering*, vol. 29, no. 6, pp. 1642 – 1652.

Demerdash, N.; Gillott, D. (1974): A new approach for determination of eddy current and flux penetration in nonlinear ferromagnetic materials. *IEEE Transaction on Magnetics*, vol. 10, no. 3, pp. 682–685.

Favennec, Y.; Labbe, V.; Tillier, Y.; Bay, F. (2002): Identification of magnetic parameters by inverse analysis coupled with finite-element modeling. *IEEE Transaction on Magnetics*, vol. 38, no. 6, pp. 3607–3619.

Ferretti, E. (2003): Crack propagation modeling by remeshing using the cell method (cm). *Computer Modeling in Engineering & Science*, vol. 4, pp. 51–72.

Ferretti, E. (2009): Cell method analysis of crack propagation in tensioned concrete plates. *Computer Modeling in Engineering & Sciences*, vol. 54, no. 3, pp. 253–282.

Freschi, F.; Giaccone, L.; Repetto, M. (2008): Educational value of the algebraic numerical methods in electromagnetism. *COMPEL - The International Journal for Computation and Mathematics in Electrical and Electronic Engineering*, vol. 27, no. 6, pp. 1343–1357.

Freschi, F.; Repetto, M. (2012): *Scientific Computing in Electrical Engineering*, chapter Tonti diagrams and algebraic methods for the solution of coupled problems, pp. 195–203. Springer Berlin Heidelberg, 2012.

Hantila, F. (1999): Electromagnetic field in non-linear media. *Balkan Journal of Geometry and its Applications*, vol. 4, no. 2, pp. 49–62.

Moro, E.; Alotto, P.; Freschi, F.; Guarnieri, M. (2012): A cell method formulation of 3-D electrothermomechanical contact problems with mortar discretization. *IEEE Transactions on Magnetics*, vol. 42, no. 2, pp. 503–506.

Paoli, G.; Bíró, O.; Buchgraber, G. (1998): Complex representation in nonlinear time harmonic eddy current problems. *IEEE Transaction on Magnetics*, vol. 34, no. 5, pp. 2625–2628.

Repetto, M.; Trevisan, F. (2004): Global formulation for 3D magneto-static using flux and gauged potential approaches. *Int. Journal on Numerical Methods in Engineering*, vol. 60, pp. 755–772.

Specogna, R.; Trevisan, F. (2005): Discrete constitutive equations in $a - \chi$ geometric eddy-current formulation. *IEEE Transactions on Magnetics*, vol. 41, no. 4, pp. 1259–1263.

Specogna, R.; Trevisan, F. (2008): Eddy-currents computation with $t-\omega$ discrete geometric formulation for a NDE problem. *IEEE Transactions on Magnetics*, vol. 44, no. 6, pp. 698–701.

Straface, S.; Troisi, S.; Gagliardi, V. (2006): Application of the cell method to the simulation of unsaturated flow. *Computers, Materials & Continua*, vol. 3, no. 3, pp. 155–166.

Tonti, E. (2001): A direct discrete formulation of field laws: The cell method. *Computer Modeling in Engineering & Sciences*, vol. 2, no. 2, pp. 237–258.

Tonti, E. (2002): Finite Formulation of Electromagnetic Field. *IEEE Transactions on Magnetics*, vol. 38, pp. 333–336.

Tonti, E.; Zarantonello, F. (2009): Algebraic formulation of elastostatics: the cell method. *Computer Modeling in Engineering & Sciences*, vol. 39, no. 3, pp. 201 – 236.

Tonti, E.; Zarantonello, F. (2010): Algebraic formulation of elastodynamics: the cell method. *Computer Modeling in Engineering & Sciences*, vol. 64, no. 1, pp. 37–70.

Vassent, E.; Meunier, G.; Sabonnadier, J. (1989): Simulation of induction machine operation using complex magnetodynamic finite elements. *IEEE Transaction on Magnetics*, vol. 25, no. 4, pp. 3064–3066.

